

Article

Photo-Induced Preparation of Ag@MOF-801 Composite Based Heterogeneous Nanocatalyst for the Production of Biodiesel

Osamah M. Alduhaish *, Mohammed Rafi Shaik  and Syed Farooq Adil *

Department of Chemistry, College of Science, King Saud University, P.O. Box 2455, Riyadh 11451, Saudi Arabia; mrshaik@ksu.edu.sa

* Correspondence: oalduhaish@ksu.edu.sa (O.M.A.); sfadil@ksu.edu.sa (S.F.A.); Tel.: +966-11-46-70439 (S.F.A.)

Abstract: Hybrid materials based on metal-organic frameworks (MOFs) and nanoparticles (NPs) have gained considerable popularity in a variety of applications. Particularly, these types of materials have demonstrated excellent efficiency in heterogeneous catalysis due to the synergistic effect between the components. Herein, we report a simple, eco-friendly, photocatalytic method for the fabrication of Zr containing MOF-801 and a silver (Ag) NPs-based hybrid (Ag@MOF-801). In this method, the photocatalytic property of the central metal ion (Zr) of MOF was exploited to promote the formation and deposition of Ag NPs on the surface of the MOF-801 under the irradiation of visible light. The successful incorporation of Ag NPs was ascertained by powder X-ray diffraction (XRD) and UV-Vis analysis, while the morphology and surface area of the sample was determined by N₂ adsorption-desorption and scanning electron microscopy (SEM), respectively. The resulting Ag@MOF-801 hybrid served as a highly efficient catalyst for the transesterification of used vegetable oil (UVO) for the production of biodiesel. The Ag@MOF-801 catalyst exhibited superior catalytic activity compared to its pristine MOF-801 counterpart due to the enhanced surface area of the material.

Keywords: metal-organic framework; Zr-fumarate-MOF; Ag nanoparticles; nanocatalyst; biodiesel



Citation: Alduhaish, O.M.; Shaik, M.R.; Adil, S.F. Photo-Induced Preparation of Ag@MOF-801 Composite Based Heterogeneous Nanocatalyst for the Production of Biodiesel. *Catalysts* **2022**, *12*, 533. <https://doi.org/10.3390/catal12050533>

Academic Editor: Ewa Kowalska

Received: 4 April 2022

Accepted: 5 May 2022

Published: 11 May 2022

Publisher's Note: MDPI stays neutral with regard to jurisdictional claims in published maps and institutional affiliations.



Copyright: © 2022 by the authors. Licensee MDPI, Basel, Switzerland. This article is an open access article distributed under the terms and conditions of the Creative Commons Attribution (CC BY) license (<https://creativecommons.org/licenses/by/4.0/>).

1. Introduction

MOFs are metal ions and multifunctional organic ligands based on crystalline, porous materials, which have gained significant attention from researchers worldwide [1,2]. They possess a unique 3D structure formed by the self-assembly of metal ions with multi-dentate organic ligands via coordination bonds. Owing to their novel properties, these materials are extensively used in a variety of applications such as gas separation, chemical sensing, biomedical and catalytic applications, etc. [3–5]. Particularly, due to their easy customization by the variation of metal ions and linkers and further modifications via post-synthesis processes, MOFs offer extraordinary structure flexibility [6,7]. In addition, due to their highly porous structure, MOF-based materials offer an ultra-high surface area (10,000 m²g⁻¹), which is considerably higher than carbonaceous materials and zeolites; hence, MOFs are also considered excellent catalyst templates [8,9]. The central metal ions in MOFs offer coordinatively unsaturated metal sites which act as superb Lewis acid catalysts either by themselves or due to the synergistic effect with inserted materials such as metallic nanoparticles (NPs), etc. [10,11].

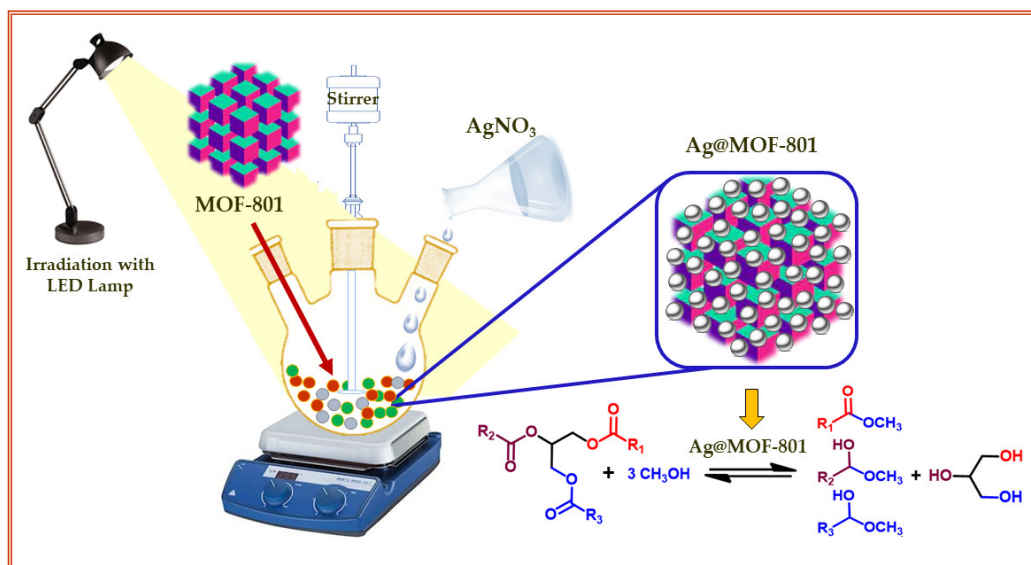
Furthermore, additional catalytically active metal sites can be introduced in MOFs by the metalation of organic ligands either during the synthesis of MOFs or by the post-synthesis modifications [12,13]. Currently, MOFs are already established as efficient catalytic materials due to their variety of topologies and the possibility of combining them with other guest materials such as metal, metal oxide NPs, carbon materials, etc. [14–17]. The deposition of NPs in MOFs during post-synthesis modifications facilitates the growth of ultra-fine nanomaterials, and the functional groups of organic ligands prevent the leaching of catalytically active material, which significantly enhances the catalytic activity of

MOF-based nanocatalysts [18,19]. Furthermore, the insolubility of MOFs in organic solvents makes them ideal catalysts in heterogeneous catalysis, and the uniform pore sizes and shapes in MOFs can be exploited in size-selective catalysis [20,21].

Due to this, the trend of combining MOFs with other materials, especially metal and metal oxide NPs, has gained considerable attention to enhance the intrinsic properties of MOFs, such as surface area, thermal, electrical, and electronic properties and so on [21]. MOFs are efficient in supporting materials when compared to other porous materials due to their novel 3D pore matrices and organic ligands, which facilitate the stabilization of NPs during their growth [22]. Often, the central metal ion and organic linkers act in synergy with the guest NPs resulting in the enhanced activity of the composite [23]. So far, significant efforts were devoted to producing high-quality MOF-NP-based nanocomposites using a variety of methods, including the liquid impregnation method, solid grinding, chemical vapor deposition (CVD), etc. [24,25]. Among these methods, the impregnation method is most commonly applied, which involves the reduction of a metal precursor using a reducing agent to produce NPs.

However, there are several issues that limit the applications of these methods [26,27]. For example, the CVD method requires volatile metal precursors and complicated operating conditions, whereas the reduction methods involve the use of high temperatures, harsh reducing agents, additional stabilizing ligands, etc. [23]. Recently, to overcome these issues, MOF-NP-based composites were fabricated by the simultaneous irradiation of UV and/or visible light on the metal precursors and photoactive MOFs [28]. Using these methods, NPs can be specifically deposited in the targeted area of MOFs [29]. Upon irradiation, electrons in the valence band of the central metal ion of semiconducting MOFs are excited to the conduction band, which facilitates the reduction of the metal precursor leading to the deposition of NPs in the resulting composite [30,31]. Using this method, different types of NPs, including Pt, Au and Pd, etc., are deposited on semiconducting MOFs such as TiO₂-based MIL-125, which has demonstrated enhanced photocatalytic activity due to the incorporation of NPs [32,33]. Apart from this, various MOFs consisting of other photoactive central metal ions, such as Zn, Fe, Zr, etc., are also exploited for the photocatalytic deposition of NPs [24].

Among these photocatalytically active MOFs, Zr-based MOFs have gained decent attention due to their higher stability [34]. Recently, we published the preparation and catalytic properties of Zr-fumarate-MOF, which is also referred to as MOF-801 [35]. In order to exploit the decent photocatalytic properties of Zr-based MOFs, in the present research, we report a simple and eco-friendly photocatalytic method to produce MOF-801 and Ag hybrids (Ag@MOF-801). To the best of our knowledge, the MOF-801 has never been used to produce the reported hybrid using the photocatalytic method. In this method, the central Zr ion of MOF-801 facilitated the reduction of AgNO₃ upon irradiation with visible light. In addition, the as-prepared hybrid effectively catalyzed the transesterification reaction of used vegetable oil (UVO) for the production of biodiesel (Scheme 1). Compared to the parent MOF-801, the as-prepared hybrid MOF-801@Ag demonstrated a decent improvement in the catalytic behavior due to the enhancement of the surface area of the material.



Scheme 1. Graphical representation of transesterification of UVO to biodiesel utilizing the synthesized MOF-801 and silver (Ag) NPs based hybrid (Ag@MOF-801) catalyst.

2. Results and Discussions

2.1. X-ray Powder Diffraction (XRD) Analysis

The Ag NPs were deposited on MOF-801 (freshly prepared according to our previously published study [35]), using AgNO₃ as a precursor. In this eco-friendly approach, the visible light source and photocatalytic properties of the central metal ion (Zr) of MOF were exploited to promote the successful reduction of metal precursors to produce the Ag@MOF-801 hybrid. Initially, the formation of MOF-801 was confirmed by matching the XRD pattern of as-prepared MOF (cf. Figure 1) with the published data. When compared, as shown in Figure 1, the XRD pattern of Ag@MOF-801 consists of several additional reflections apart from the characteristic reflections of MOF-801, i.e., the reflections at $\sim 10^\circ$, 13.9° , 19.9° , and 21.7° , which are assigned to the (200), (222), (420), and (440) planes. The additional reflections which appeared at $\sim 37.5^\circ$, 44.1° , 64.3° , 79.3° , and 81.2° , are the characteristic reflections of Ag NPs belonging to the (111), (200), (220), (311), and (222) Miller indices (Khan et al., 2013). This confirms the formation of a highly crystalline, face-centered cubic (fcc) structure of the Ag NPs on MOF-801.

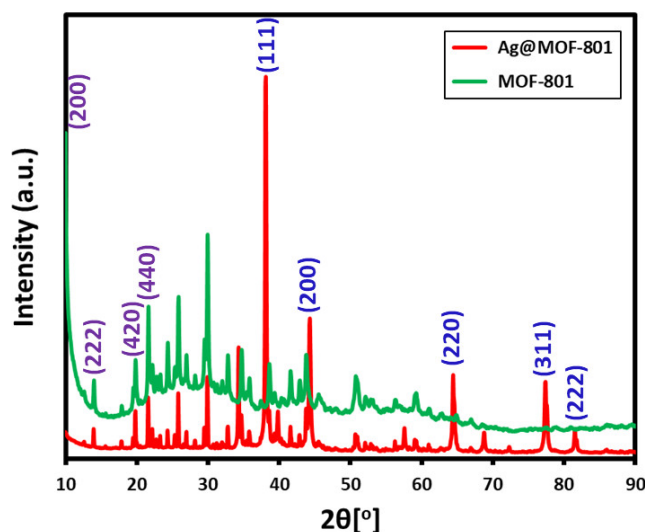


Figure 1. XRD analysis of MOF-801 and Ag@MOF-801.

2.2. SEM and EDX Analysis of Ag@MOF-801

The structural details of the Ag@MOF-801 hybrid was ascertained by FESEM. As shown in Figure 2a, the SEM image of the hybrid depicts the presence of an octahedral shape material belonging to the MOF-801. On the other hand, the surface of the octahedra is covered by well-distributed spherical shape particles, which indicates the presence of Ag NPs on the surface of MOF. The presence of Ag in the sample is further confirmed by the elemental analysis using EDX. The EDX spectrum in Figure 2b exhibited a characteristic Ag peak at ~3 keV, which confirmed the presence of silver in the sample. Apart from this, the spectrum also showed the presence of Zr, C, and O, which are represented by the intense peak of Zr at 2.1 keV and relatively smaller peaks at ~0.28 and 0.55 keV for C and O, respectively. These peaks pointed toward the presence of MOF-801 in the sample.

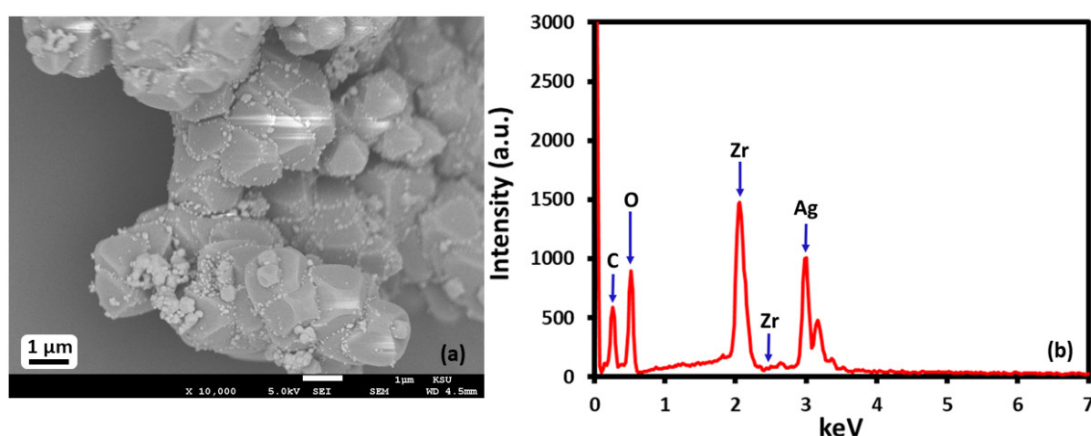


Figure 2. (a) SEM and (b) EDX analysis of Ag@MOF-801.

2.3. UV-Visible and Fourier-Transform Infrared Spectroscopy Analysis

The formation of Ag NPs can also be confirmed by the UV analysis; typically, Ag displays a distinct peak between 380–470 nm depending on the size and shape of NPs, due to the localized surface plasmon resonance effect [36]. In this case, the UV spectrum of Ag@MOF-801 shown in Figure 3a also exhibits an absorption peak at ~450 nm, which points toward the formation of Ag NPs in the sample. Furthermore, FT-IR analysis was performed to investigate the chemical interactions between deposited Ag NPs with the chemical functionalities of MOF-801. As shown in Figure 3b, the IR spectrum of Ag@MOF-801 exhibited prominent peaks at the characteristic positions which are almost identical to the peaks of pristine MOF-801 [35]. For instance, a broad OH peak at $\sim 3400\text{ cm}^{-1}$, C=O stretching peak at 1650 cm^{-1} , O–C–O asymmetric stretching peak of the carboxylic group at 1578 cm^{-1} , the symmetrical and asymmetrical stretching peak of C–H between $3100\text{--}2800\text{ cm}^{-1}$, etc. Indeed, the characteristic sharp vibration peaks of $\text{Zr}_6(\text{OH})_4\text{O}_4$, and asymmetric stretching of the Zr-(OC) group also appeared at the same positions, i.e., at 655 and 491 cm^{-1} . This clearly indicated that the Ag NPs are physically adsorbed on the surface of pristine MOF-801 and do not interact chemically with the ligands and the central ion of pristine MOF. For catalytic applications, the surface area of the material plays a critical role in enhancing the catalytic properties. N_2 adsorption-desorption isotherm analyses were conducted to identify the Brunauer-Emmett-Teller (BET) specific surface area and Barrett-Joyner-Halenda (BJH) pore size distribution of Ag@MOF-801. While the pristine MOF-801 itself demonstrated a high BET surface area of $750.11\text{ m}^2/\text{g}$, its metallic NPs modified hybrid counterpart (Ag@MOF-801) showed a more enhanced BET surface area of $827.70\text{ m}^2/\text{g}$ (cite our crystal paper here). This can be attributed to the presence of Ag NPs on the surface of MOF, as the size of the micropores remained unaffected with the pores' distribution mostly microporous (Figure 4a), which is similar to the pore size of pure MOF-801 as shown in Figure 4b.

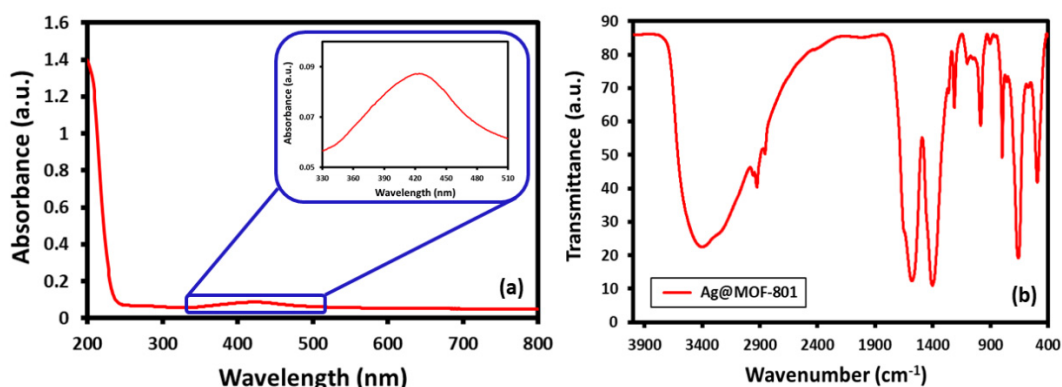


Figure 3. (a) UV-Visible and (b) FT-IR analysis of Ag@MOF-801.

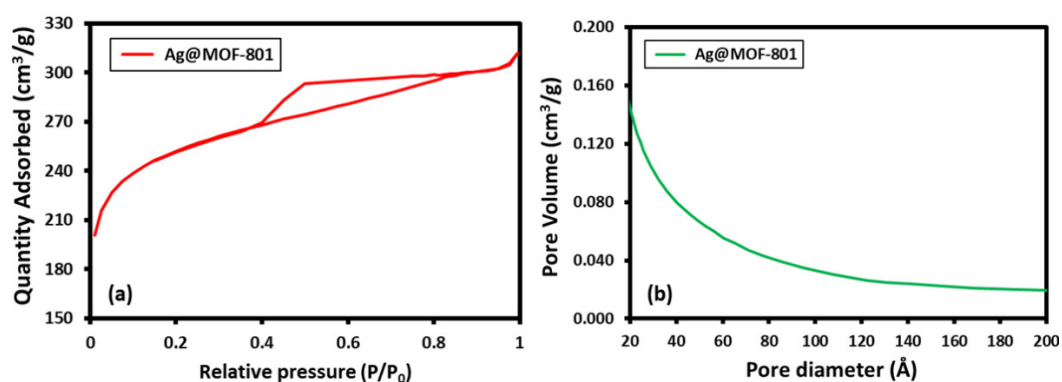


Figure 4. (a) N₂ adsorption-desorption isotherm and (b) pore size distribution of Ag@MOF-801.

2.4. Catalytic Evaluation of Ag@MOF-801

To ascertain the catalytic properties of Ag@MOF-801, the hybrid was applied as a catalyst in the transesterification of used vegetable oil (UVO). In our previously published study, the MOF-801 was used to catalyze a similar reaction, where the progress of the reaction was tracked via ¹H NMR spectroscopy. In this case, the yield of the product (glycerol) is analyzed by NMR, ultimately indicating the amount of conversion of UVO. To begin with, several transesterification reactions were performed by varying the amount of Ag@MOF-801 catalyst. Reactions were carried out at 180 °C for 8 h using a mixture of oil (as reactant) and methanol (50 wt%). Throughout these reactions, the conditions remained the same, except for the amount of catalyst; further details are provided in Table 1. Results of the NMR analysis confirming the conversion of UVO are provided in the Supplementary File Figure S1. Similar to the results obtained in the case of pristine MOF-801, in this case, 10 wt% of the catalyst with respect to the amount of oil offered maximum conversion (~70.1%). However, the Ag@MOF-801 hybrid catalyst demonstrated higher catalytic activity compared to its pristine counterpart, which rendered only ~60% conversion when the same amount of catalyst was used (cite our crystal paper here). The enhanced catalytic property of the Ag@MOF-801 hybrid can be attributed to the increased surface area of the catalyst. Notably, upon adjusting the pH of the reaction with the addition of HCl (10% *v/v*), the yield of the reaction further increased to more than 73.1%; this can be ascribed to the inherent catalytic property of HCl towards the esterification reaction [37]. Expectedly, the variation of the quantity of the catalyst between 10–20 wt.% has little effect on the amount of conversion, as the yield of the product slightly decreased up to ~3% (Figure 5a). On the other hand, using a smaller amount of catalyst, lower than 10 wt% (5 wt%), significantly decreased the quantity of the product and rendered only ~43% of yield (cf. Table 1). Furthermore, several experiments were carried out to optimize the time and temperature of the reactions. As appeared in the case of pristine MOF-801, herein

also 8 h of reaction time rendered maximum conversion (~70.1%), while less reaction time produced a lower reaction yield (cf. Figure 5b). Likewise, a temperature of 180 °C produced maximum conversion, while below this temperature, less amount of product was obtained (cf. Figure 6a). Furthermore, the reusability tests of the Ag@MOF-801 performed under optimized reaction conditions revealed the decent stability of the catalyst up to three cycles, during which the yield of products slightly decreased (only up to ~8%) (cf. Figure 6b).

Table 1. The transesterification reactions of UVO in methanol using different amounts of oil.

Catalyst	Oil (g)	Amount of Catalyst		Product Yield (g)		Conversion (%)	
		Wt. % to Oil	Amount (g)	Biodiesel	Glycerol	¹ H-NMR	Yield of Glycerol
Ag@MOF-801	1.5	5	0.075	1.334	0.058	42.5	37.4
Ag@MOF-801		10	0.150	1.423	0.107	70.1	69.0
Ag@MOF-801		15	0.225	1.419	0.105	69.5	67.7
Ag@MOF-801		20	0.300	1.416	0.101	67.5	65.2
Ag@MOF-801/HCl		10	0.150	1.491	0.124	73.1	72.9

Reaction conditions: Temperature—180 °C, Methanol to oil (50 wt%), and time 8 h.

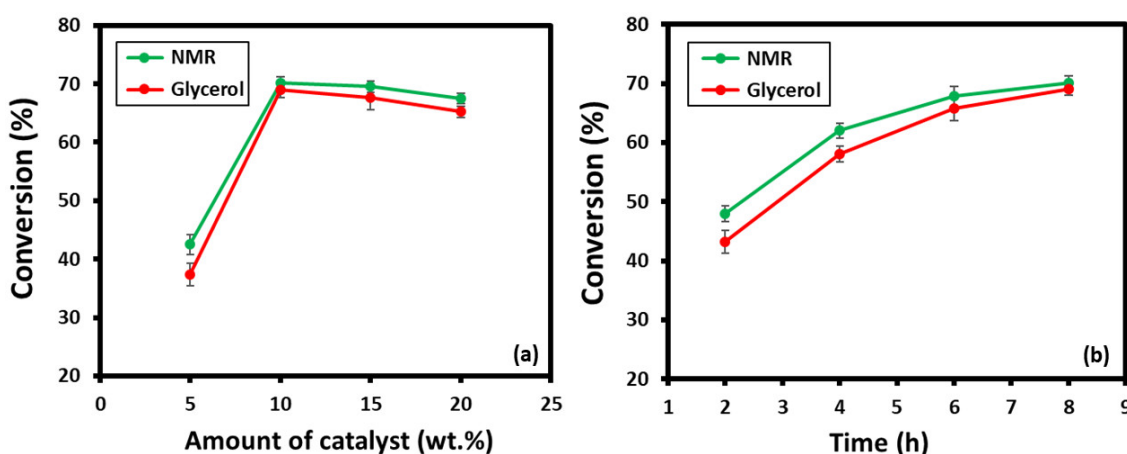


Figure 5. Conversion of UVO in the presence of Ag@MOF-801 as catalysts using different reaction parameters (a) at varying catalyst loading (green line conversion based on NMR and red line conversion based on the yield of glycerol) and (b) at a different time interval.

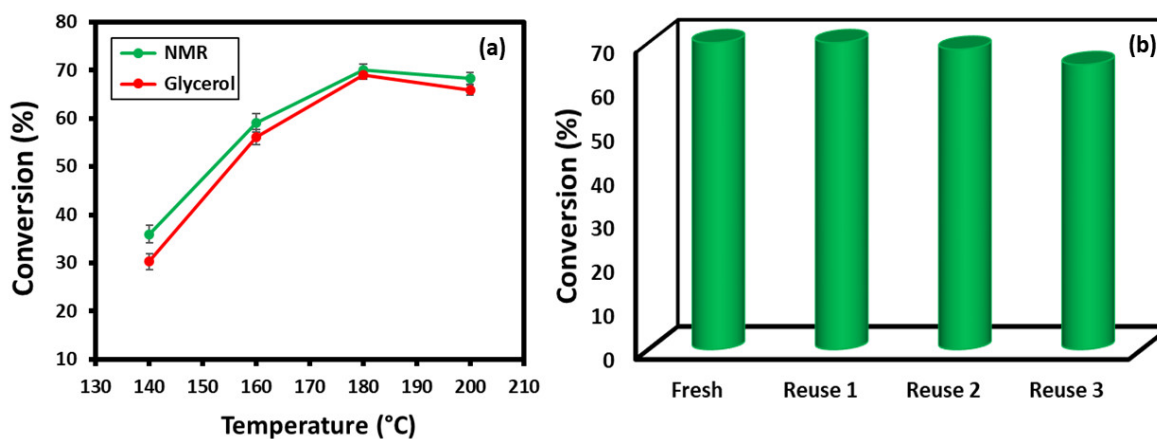


Figure 6. Transesterification of UVO over Ag@MOF-801, (a) at different temperatures and (b) reusability study of the Ag@MOF-801.

2.5. Mechanism of Biodiesel Production Using Ag@MOF-801

The components of biodiesel involve a series of fatty acid alkyl esters (FAAE) which are formed by the transesterification of triglycerides typically present in the vegetable oils (UVO) and animal fats, etc. The high contents of free fatty acid (FFA) present in UVO is typically removed via esterification reaction, where FFAs react with alcohol to produce FAAE and water [38]. In other words, esterification reduces the acid content of feedstock oil for transesterification. For both esterification and transesterification reactions, catalysts are required (homogenous and/or heterogeneous catalysts) to achieve effective conversion. Heterogeneous catalysts are further divided into two categories: acidic and basic, and the mechanism of the transesterification reactions varies according to the variety of catalysts [39]. In this study, Ag@MOF-801 is applied as a heterogeneous catalyst; the MOF-based catalysts are categorized based on the types of organic ligands, which usually involve carboxylic acid-based ligands, nitrogen heterocyclic rings based ligands, and other ligands (Figure 7) [40,41]. The Ag@MOF-801 consists of dicarboxylic acid (fumaric acid) as an organic ligand which makes it an acidic heterogeneous catalyst. In the case of an acid catalyst, the mechanism of transesterification initially involves the protonation of carbonyl of the carboxylic acid. Subsequently, the positive charge of carbonyl carbon facilitates the nucleophilic reaction of alcohol with the formation of intermediates. Thereafter, the proton is transferred with the removal of water, which is finally eliminated with the formation of ester. In the case of Ag@MOF-801, the reaction may occur in the following steps, (i) CH₃OH coordinates with the central Zr atoms of the MOF-801, (ii) triglyceride of UVO attach to the Zr atom of the MOF-801, (iii) the nucleophilic oxygen atom from methanol then attacks the electrophilic carbon at the triglyceride ester group which facilitates transesterification, this nucleophilic attack produces glycerol by-product, (iv) finally, FAAE (biodiesel) detach from the MOF through electron delocalization at the oxygen atoms to produce biodiesel [42].

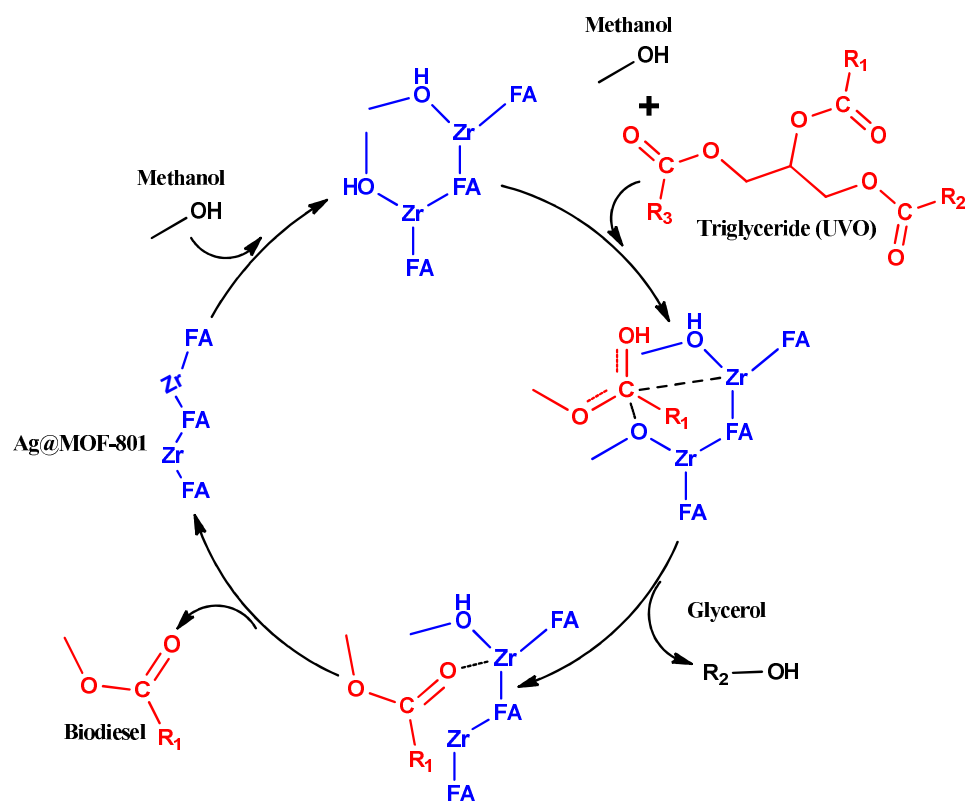


Figure 7. Tentative mechanism of transesterification reaction of UVO for the production of biodiesel using Ag@MOF-801 catalyst; (Zr-Zirconium; FA-Fumaric acid).

3. Materials and Methods

3.1. Materials

Zirconium (IV) oxychloride octahydrate ($\text{ZrOCl}_2 \cdot 8\text{H}_2\text{O}$), silver nitrate (AgNO_3), fumaric acid, dimethylformamide (DMF), formic acid, ethanol, methanol, and hexane were purchased from Sigma-Aldrich, St. Louis, MO 68178, USA. Used vegetable oil was obtained from a fast-food center in Riyadh, Saudi Arabia.

3.2. Sample Preparation (Ag@MOF-801)

All reagents and solvents were procured from commercial sources and used as received without any further purification. MOF-801 was produced according to our previously published study [35]. For the preparation of Ag@MOF-801 hybrid (50 wt% of silver), an aqueous solution of AgNO_3 (100 mg dissolved in 2.5 mL water) was first prepared. Separately, 200 mg of freshly prepared MOF-801 were dispersed in 25 mL ethanol via gentle stirring at room temperature for 30 min. Thereafter, the aqueous solution of AgNO_3 was added to the ethanol dispersion, and the mixture was gradually heated (increased the heat slowly, $10\text{ }^\circ\text{C}$ every 10 min) to $80\text{ }^\circ\text{C}$. Once the temperature reached $80\text{ }^\circ\text{C}$, the mixture was irradiated with a 24 W Philips light-emitting diode (LED) lamp ($\lambda > 400\text{ nm}$). The lamp was placed at a distance of $\sim 10\text{ cm}$ from the reaction flask; meanwhile, the mixture was continuously stirred until the color of the mixture changed to light brown ($\sim 30\text{ min}$). After this, the reaction was stopped, and the product was isolated via centrifugation; a light brown powder was obtained, which was further washed three times with a mixture of water and ethanol (1:1) to remove the unreacted Ag precursor. Finally, a brown powder was obtained, which was then dried at $70\text{ }^\circ\text{C}$ in an oven overnight to derive the Ag@MOF-801 hybrid. The experimental details of the conversion of UVO to esters and the details about the confirmation of the formation of the product via $^1\text{H NMR}$ are provided in the Supplementary information. Furthermore, the Supplementary File also includes all the details about sample preparation for characterization and other technical information about the instruments used during this study.

3.3. Transesterification of Used Vegetables Oil (UVO) Using Ag@MOF-801

The transesterification of used vegetables oil (UVO) using the Ag@MOF-801 procedure is provided in the Supplementary File.

3.4. Characterization

Characterization details are provided in the Supplementary File.

4. Conclusions

In summary, we presented a highly efficient, eco-friendly photocatalytic method for the preparation of MOF-801 and a Ag NP-based Ag@MOF-801 hybrid. The hybrid was prepared by utilizing the efficient photocatalytic properties of the central Zr ion of MOF-801. The central ion facilitated the reduction of the metal precursor under visible light irradiation leading to the successful deposition of Ag NPs on the surface of MOF. The presence of Ag NPs enhanced the surface area of the hybrid catalyst, due to which the resulting nanocatalyst demonstrated superior catalytic properties when compared to its parent material, towards the esterification of UVO for the production of biodiesel. Therefore, the protocol demonstrated here for the preparation of Ag@MOF-801 can be further extended to prepare other MOFs-NPs composites by utilizing the photocatalytic properties of semiconducting central ions-based MOFs.

Supplementary Materials: The following supporting information can be downloaded at: <https://www.mdpi.com/article/10.3390/catal12050533/s1>. Figure S1: SEM analysis of MOF-801; Figure S2: FT-IR analysis of MOF-801.

Author Contributions: O.M.A.: conceptualization, visualization, resources, supervision, writing—review and editing, funding acquisition; M.R.S.: investigation, formal analysis, writing—original draft

preparation, data curation; S.F.A.: investigation, visualization, validation, methodology, writing—review and editing. All authors have read and agreed to the published version of the manuscript.

Funding: The authors extend their appreciation to the Deputyship for Research & Innovation, Ministry of Education in Saudi Arabia for funding this research work through the project number (DRI-KSU-572).

Data Availability Statement: Not applicable.

Acknowledgments: The authors extend their appreciation to the Deputyship for Research & Innovation, Ministry of Education in Saudi Arabia for funding this research work through the project number (DRI-KSU-572).

Conflicts of Interest: The authors declare no conflict of interest.

References

1. Stock, N.; Biswas, S. Synthesis of metal-organic frameworks (MOFs): Routes to various MOF topologies, morphologies, and composites. *Chem. Rev.* **2012**, *112*, 933–969. [[CrossRef](#)] [[PubMed](#)]
2. Zhou, H.-C.; Long, J.R.; Yaghi, O.M. Introduction to metal-organic frameworks. *Chem. Rev.* **2012**, *112*, 673–674. [[CrossRef](#)] [[PubMed](#)]
3. Chen, L.; Zhang, X.; Cheng, X.; Xie, Z.; Kuang, Q.; Zheng, L. The function of metal-organic frameworks in the application of MOF-based composites. *Nanoscale Adv.* **2020**, *2*, 2628–2647. [[CrossRef](#)]
4. Lian, X.; Fang, Y.; Joseph, E.; Wang, Q.; Li, J.; Banerjee, S.; Lollar, C.; Wang, X.; Zhou, H.-C. Enzyme-MOF (metal-organic framework) composites. *Chem. Soc. Rev.* **2017**, *46*, 3386–3401. [[CrossRef](#)]
5. Chen, J.; Zhu, Y.; Kaskel, S. Porphyrin-Based Metal-Organic Frameworks for Biomedical Applications. *Angew. Chem. Int. Ed.* **2021**, *60*, 5010–5035. [[CrossRef](#)]
6. Mandal, S.; Natarajan, S.; Mani, P.; Pankajakshan, A. Post-Synthetic Modification of Metal-Organic Frameworks Toward Applications. *Adv. Funct. Mater.* **2021**, *31*, 2006291. [[CrossRef](#)]
7. Liu, M.; Liang, J.; Tian, Y.; Liu, Z. Post-synthetic modification within MOFs: A valuable strategy for modulating their ferroelectric performance. *CrystEngComm* **2022**, *24*, 724–737. [[CrossRef](#)]
8. Wang, Q.; Astruc, D. State of the art and prospects in metal-organic framework (MOF)-based and MOF-derived nanocatalysis. *Chem. Rev.* **2019**, *120*, 1438–1511. [[CrossRef](#)]
9. Khan, M.; Tahir, M.N.; Adil, S.F.; Khan, H.U.; Siddiqui, M.R.H.; Al-warthan, A.A.; Tremel, W. Graphene based metal and metal oxide nanocomposites: Synthesis, properties and their applications. *J. Mater. Chem. A* **2015**, *3*, 18753–18808. [[CrossRef](#)]
10. Yu, J.; Mu, C.; Yan, B.; Qin, X.; Shen, C.; Xue, H.; Pang, H. Nanoparticle/MOF composites: Preparations and applications. *Mater. Horiz.* **2017**, *4*, 557–569. [[CrossRef](#)]
11. Song, Z.; Zhang, L.; Doyle-Davis, K.; Fu, X.; Luo, J.L.; Sun, X. Recent advances in MOF-derived single atom catalysts for electrochemical applications. *Adv. Energy Mater.* **2020**, *10*, 2001561. [[CrossRef](#)]
12. Manna, K.; Zhang, T.; Lin, W. Postsynthetic metalation of bipyridyl-containing metal-organic frameworks for highly efficient catalytic organic transformations. *J. Am. Chem. Soc.* **2014**, *136*, 6566–6569. [[CrossRef](#)] [[PubMed](#)]
13. Yuan, S.; Chen, Y.P.; Qin, J.; Lu, W.; Wang, X.; Zhang, Q.; Bosch, M.; Liu, T.F.; Lian, X.; Zhou, H.C. Cooperative cluster metalation and ligand migration in zirconium metal-organic frameworks. *Angew. Chem. Int. Ed.* **2015**, *54*, 14696–14700. [[CrossRef](#)] [[PubMed](#)]
14. Lang, X.; Wang, X.; Liu, Y.; Cai, K.; Li, L.; Zhang, Q. Cobalt-based metal organic framework (Co-MOFs)/graphene oxide composites as high-performance anode active materials for lithium-ion batteries. *Int. J. Energy Res.* **2021**, *45*, 4811–4820. [[CrossRef](#)]
15. Subudhi, S.; Tripathy, S.P.; Parida, K. Metal oxide integrated metal organic frameworks (MO@MOF): Rational design, fabrication strategy, characterization and emerging photocatalytic applications. *Inorg. Chem. Front.* **2021**, *8*, 1619–1636. [[CrossRef](#)]
16. Buasakun, J.; Srilaoong, P.; Rattanakam, R.; Duangthongyou, T. Synthesis of Heterostructure of ZnO@MOF-46 (Zn) to Improve the Photocatalytic Performance in Methylene Blue Degradation. *Crystals* **2021**, *11*, 1379. [[CrossRef](#)]
17. Jiang, D.; Wei, C.; Zhu, Z.; Xu, X.; Lu, M.; Wang, G. Preparation of Flower-Like Nickel-Based Bimetallic Organic Framework Electrodes for High-Efficiency Hybrid Supercapacitors. *Crystals* **2021**, *11*, 1425. [[CrossRef](#)]
18. Zhu, K.; Chen, C.; Lu, S.; Zhang, X.; Alsaedi, A.; Hayat, T. MOFs-induced encapsulation of ultrafine Ni nanoparticles into 3D N-doped graphene-CNT frameworks as a recyclable catalyst for Cr(VI) reduction with formic acid. *Carbon* **2019**, *148*, 52–63. [[CrossRef](#)]
19. Karve, V.V.; Sun, D.T.; Trukhina, O.; Yang, S.; Oveisi, E.; Luterbacher, J.; Queen, W.L. Efficient reductive amination of HMF with well dispersed Pd nanoparticles immobilized in a porous MOF/polymer composite. *Green Chem.* **2020**, *22*, 368–378. [[CrossRef](#)]
20. Zhang, W.; Lu, G.; Cui, C.; Liu, Y.; Li, S.; Yan, W.; Xing, C.; Chi, Y.R.; Yang, Y.; Huo, F. A family of metal-organic frameworks exhibiting size-selective catalysis with encapsulated noble-metal nanoparticles. *Adv. Mater.* **2014**, *26*, 4056–4060. [[CrossRef](#)]
21. Dhakshinamoorthy, A.; Garcia, H. Catalysis by metal nanoparticles embedded on metal-organic frameworks. *Chem. Soc. Rev.* **2012**, *41*, 5262–5284. [[CrossRef](#)] [[PubMed](#)]

22. Rivera-Torrente, M.; Filez, M.; Hardian, R.; Reynolds, E.; Seoane, B.; Coulet, M.V.; Oropeza Palacio, F.E.; Hofmann, J.P.; Fischer, R.A.; Goodwin, A.L.; et al. Metal-Organic Frameworks as Catalyst Supports: Influence of Lattice Disorder on Metal Nanoparticle Formation. *Chem. Eur. J.* **2018**, *24*, 7498–7506. [[CrossRef](#)] [[PubMed](#)]
23. Moon, H.R.; Lim, D.-W.; Suh, M.P. Fabrication of metal nanoparticles in metal–organic frameworks. *Chem. Soc. Rev.* **2013**, *42*, 1807–1824. [[CrossRef](#)] [[PubMed](#)]
24. Yu, X.; Wang, L.; Cohen, S.M. Photocatalytic metal–organic frameworks for organic transformations. *CrystEngComm* **2017**, *19*, 4126–4136. [[CrossRef](#)]
25. Li, B.; Ma, J.G.; Cheng, P. Integration of metal nanoparticles into metal–organic frameworks for composite catalysts: Design and synthetic strategy. *Small* **2019**, *15*, 1804849. [[CrossRef](#)]
26. Singh, B.K.; Lee, S.; Na, K. An overview on metal-related catalysts: Metal oxides, nanoporous metals and supported metal nanoparticles on metal organic frameworks and zeolites. *Rare Met.* **2020**, *39*, 751–766. [[CrossRef](#)]
27. Lo, W.-S.; Chou, L.-Y.; Young, A.P.; Ren, C.; Goh, T.W.; Williams, B.P.; Li, Y.; Chen, S.-Y.; Ismail, M.N.; Huang, W.; et al. Probing the Interface between Encapsulated Nanoparticles and Metal–Organic Frameworks for Catalytic Selectivity Control. *Chem. Mater.* **2021**, *33*, 1946–1953. [[CrossRef](#)]
28. Wang, D.; Song, Y.; Cai, J.; Wu, L.; Li, Z. Effective photo-reduction to deposit Pt nanoparticles on MIL-100 (Fe) for visible-light-induced hydrogen evolution. *New J. Chem.* **2016**, *40*, 9170–9175. [[CrossRef](#)]
29. Doherty, C.M.; Buso, D.; Hill, A.J.; Furukawa, S.; Kitagawa, S.; Falcaro, P. Using functional nano-and microparticles for the preparation of metal–organic framework composites with novel properties. *Acc. Chem. Res.* **2014**, *47*, 396–405. [[CrossRef](#)]
30. Wang, Z.; Zhao, S.; Zhu, S.; Sun, Y.; Fang, M. Photocatalytic synthesis of M/Cu₂O (M = Ag, Au) heterogeneous nanocrystals and their photocatalytic properties. *CrystEngComm* **2011**, *13*, 2262–2267. [[CrossRef](#)]
31. Lu, Q.; Zhu, L.; Han, S.; Hou, Y.; Cao, W. Photocatalytic synthesis of gold nanoparticles using TiO₂ nanorods: A mechanistic investigation. *Phys. Chem. Chem. Phys.* **2019**, *21*, 18753–18757. [[CrossRef](#)] [[PubMed](#)]
32. Sun, D.; Liu, W.; Fu, Y.; Fang, Z.; Sun, F.; Fu, X.; Zhang, Y.; Li, Z. Noble metals can have different effects on photocatalysis over metal–organic frameworks (MOFs): A case study on M/NH₂-MIL-125 (Ti)(M = Pt and Au). *Chem. Eur. J.* **2014**, *20*, 4780–4788. [[CrossRef](#)] [[PubMed](#)]
33. Guo, J.; Wan, Y.; Zhu, Y.; Zhao, M.; Tang, Z. Advanced photocatalysts based on metal nanoparticle/metal-organic framework composites. *Nano Res.* **2021**, *14*, 2037–2052. [[CrossRef](#)]
34. Sun, D.; Li, Z. Robust Ti- and Zr-based metal-organic frameworks for photocatalysis. *Chin. J. Chem.* **2017**, *35*, 135–147. [[CrossRef](#)]
35. Shaik, M.R.; Adil, S.F.; AlOthman, Z.A.; Alduhaish, O.M. Fumarate Based Metal–Organic Framework: An Effective Catalyst for the Transesterification of Used Vegetable Oil. *Crystals* **2022**, *12*, 151. [[CrossRef](#)]
36. Al-Marri, A.H.; Khan, M.; Khan, M.; Adil, S.F.; Al-Warthan, A.; Alkhatlan, H.Z.; Tremel, W.; Labis, J.P.; Siddiqui, M.R.H.; Tahir, M.N. *Pulicaria glutinosa* extract: A toolbox to synthesize highly reduced graphene oxide-silver nanocomposites. *Int. J. Mol. Sci.* **2015**, *16*, 1131–1142. [[CrossRef](#)]
37. Kim, B.; Im, H.; Lee, J.W. In situ transesterification of highly wet microalgae using hydrochloric acid. *Bioresour. Technol.* **2015**, *185*, 421–425. [[CrossRef](#)]
38. Ma, X.; Liu, F.; Helian, Y.; Li, C.; Wu, Z.; Li, H.; Chu, H.; Wang, Y.; Wang, Y.; Lu, W. Current application of MOFs based heterogeneous catalysts in catalyzing transesterification/esterification for biodiesel production: A review. *Energy Convers. Manage.* **2021**, *229*, 113760. [[CrossRef](#)]
39. Cong, W.-J.; Nanda, S.; Li, H.; Fang, Z.; Dalai, A.K.; Kozinski, J.A. Metal–organic framework-based functional catalytic materials for biodiesel production: A review. *Green Chem.* **2021**, *23*, 2595–2618. [[CrossRef](#)]
40. Cirujano, F.; Corma, A.; i Xamena, F.L. Zirconium-containing metal organic frameworks as solid acid catalysts for the esterification of free fatty acids: Synthesis of biodiesel and other compounds of interest. *Catal. Today* **2015**, *257*, 213–220. [[CrossRef](#)]
41. Xie, W.; Wan, F. Guanidine post-functionalized crystalline ZIF-90 frameworks as a promising recyclable catalyst for the production of biodiesel via soybean oil transesterification. *Energy Convers. Manage.* **2019**, *198*, 111922. [[CrossRef](#)]
42. Pangestu, T.; Kurniawan, Y.; Soetaredjo, F.E.; Santoso, S.P.; Irawaty, W.; Yuliana, M.; Hartono, S.B.; Ismadji, S. The synthesis of biodiesel using copper based metal-organic framework as a catalyst. *J. Environ. Chem. Eng.* **2019**, *7*, 103277. [[CrossRef](#)]